ORNL/CP-94436

CONF-9704102--

Challenges for the ITER Ion Cyclotron System*

D. W. Swain, P. M. Ryan, D. J. Taylor, G. Bosia†

Oak Ridge National Laboratory, Oak Ridge, TN
†ITER Joint Central Team, Garching, Germany

Abstract. Ion cyclotron heating is one of the methods proposed for heating and for driving current in the ITER plasma. The ITER environment is significantly different from that of present-day tokamaks because of heating from neutrons and from the high radiated heat flux. In addition, the proposed 15-cm gap between the plasma separatrix and the outer wall (where the ion cyclotron antennas are located) necessitates running the antennas at relatively high values of voltage in order to couple the required power to the plasma. There are two main questions:

- Can the ion cyclotron antennas deliver the required power to the plasma?
- Can they survive in the ITER environment?

Results presented in this paper indicate that the antennas can survive both normal operation and disruptions in ITER, and can deliver the power to the plasma.

1. INTRODUCTION

The ITER ion cyclotron system must supply 50 MW of power to heat and drive current in the ITER plasma. The operating requirements will be more challenging than on present-day fusion experiments because of:

- Large (~ 15-cm) antenna-plasma separation (resulting in high voltages and currents to deliver the required power);
- Varying loading resistance (caused by plasma motion of up to ± 5 cm, transition from L-mode to H-mode, and ELMing plasmas during H-mode operation) that may require fast active matching during operation;
- Relatively high inter-strap inductive coupling and low resistive loading, which may result in operation with $kQ \approx 1$;
- High heat loads during normal operation (from radiated plasma power and neutron fluxes);

* Research sponsored by the Office of Fusion Energy, U.S. Department of Energy, under contract DE-AC05-96OR22464 with Lockheed Martin Energy Research Corporation.

DISCLAIMER

- Large disruption forces and heat loads;
- Long-pulse operation (~1000 s) and long total integrated operation time;
- A high-radiation environment, requiring remote installation and some remote maintenance of the antennas.

None of these requirements appears insurmountable. Many of the challenges cited above have already been addressed on presently operating devices, although not simultaneously. This paper will concentrate on the mechanical and electrical design of the ion cyclotron (IC) antenna and of the matching and decoupling system. After a brief overview of the ion cyclotron system, Sec. 2 will present an electrical analysis of the system, and Sec. 3 the results of thermal and stress analyses.

The ITER IC system will operate at a number of frequencies in the 30 to 70 MHz range. Figure 1 shows the resonances of different ion species vs. major radius for a magnetic field of 5.7 T on axis, and some of the proposed operating frequencies ([1]). The IC system will have antennas mounted in four main horizontal ports; Fig. 2 shows one antenna.

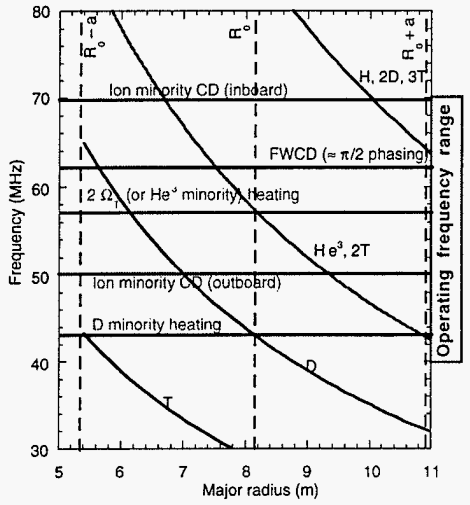

FIGURE 1. Operating frequencies.

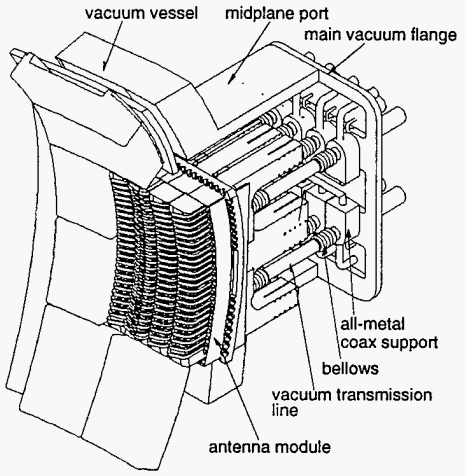

FIGURE 2. Antenna in horizontal port.

Each antenna module consists of eight current straps in a 4 (toroidal) x 2 (poloidal) array. The ends of each current strap are terminated by adjustable shorted stubs, and each strap is driven by a coax line connected near its center; this forms a resonant double loop (RDL) antenna configuration ([2]). For a given frequency and value of plasma loading resistance R', adjustment of the two stub lengths can tune the antenna to appear as a matched load to the driving source.

A schematic diagram of the circuitry driving one current strap is shown in Fig. 3. Two all-metal supports ([3]) provide mechanical support for the vacuum coax as it leaves the RDL. A vacuum window located at the main vacuum flange separates the torus vacuum from pressurized coax transmission lines. The antenna module is a single unit that can be installed and removed from a main port using remote maintenance equipment.

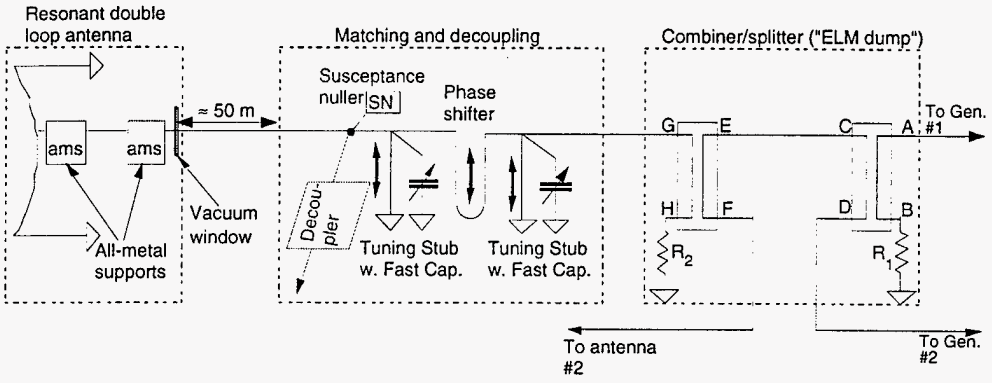

FIGURE 3. Schematic diagram of the resonant double loop, transmission lines, and matching circuitry for one current strap.

A design study has shown the potential of using fast capacitors in parallel with tuning stubs to match variable loads with a time response of ~20 ms, a technique currently employed on TEXTOR ([4]). Faster load variations (e.g., during ELM's and L-H transitions) are accepted within a large load range (2-8 Ω/m) by the antenna pre-tuning leading to relatively low input VSWR (<2.5). The matching and decoupling circuit also decouples adjacent transmission lines, to compensate for the inter-strap coupling from the mutual inductance between adjacent current straps in the antenna.

A dual hybrid combiner/splitter circuit (shown in the figure) can act as an additional protection circuit for the generators when the antenna is run with current-drive phasing of $\pi/2$ between adjacent current straps. In this case, the two generators driving terminals A and D of the first hybrid unit are operated with $\pi/2$ phasing between them, resulting in the sum of their powers through line CE. This power, split evenly between output ports F and G (with a $\pi/2$ phase difference between them) drives two adjacent current straps. In the event that power is reflected back because of a sudden change in R' (assuming that both straps see approximately the *same* change in R') the power reflected back to ports F and G will wind up in dump resistor R_2. This provides additional protection for the generators, keeping short transients of reflected power from reaching them. This circuit has been used on ASDEX-U very successfully ([5]).

2. ELECTRICAL ANALYSIS

The nominal position of the separatrix of the ITER plasma is 15 cm from the outer wall; in addition, the antenna is recessed ≈ 1 cm behind the first wall. Using a detailed model of the antenna geometry and a plasma density profile specified by the ITER Joint Central Team, the plasma load resistance R' was calculated using the RANT3D code ([6]). The plasma loading for the antenna is relatively low: for $\pi/2$ inter-strap phasing, R' varies from 2 Ω/m at 40 MHz to 7 Ω/m at 80 MHz.

Using the calculated values of R' and a lossy transmission line model for the current strap and stubs, the current and voltage in the antenna was computed. The results are shown in Fig. 4. R' increases faster than linearly with frequency,

resulting in currents and voltages on the strap being higher at lower frequencies. The maximum voltage in the antenna structure at 40 MHz is about 45 kV. This occurs in the pre-matching stub at a distance of ≈ 0.9 m from the plasma. The peak voltage *on the current strap* is ≤ 35 kV; this value is relatively independent of frequency, as can be seen from Fig. 4. Current straps in several contemporary machines operate with peak voltages ≥ 40 kV ([7]), so the operating voltages for the ITER antenna are not greatly in excess of present-day achievements.

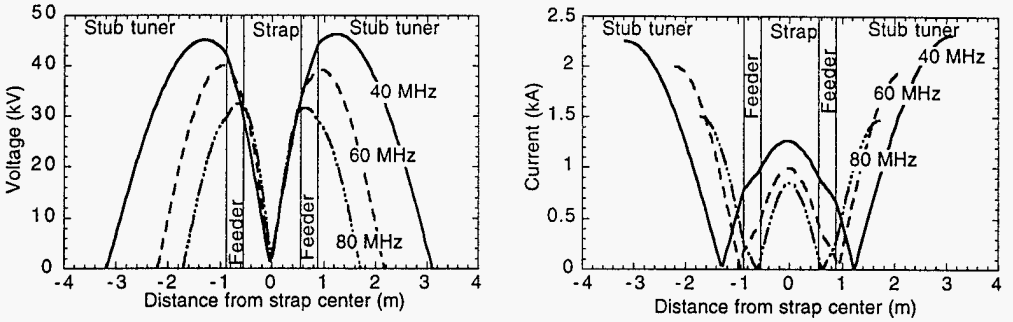

FIGURE 4. Voltage (left) and current (right) along the strap and stubs required to deliver 50 MW from four ports for 40, 60 and 80 MHz. Inter-strap phasing is π/2.

The present design of the ITER antenna has about a 6% mutual inductive coupling coefficient between adjacent current straps (which could be reduced by an increase in height of the inter-strap septa, if needed). For π/2 inter-strap phasing, this causes an imbalance in the *power* to each strap needed to drive equal strap *currents* (equal currents are desired for efficient current drive; it also results in equal voltages in the RDL circuits). For a total power of 12.5 MW/port, the power to each strap vs. R' is shown in Fig. 5.

In order to make efficient use of the generators, approximately equal power must be obtained from each generator. This can be done using simple shorted-stub decouplers indicated in Fig. 6. Shown in the figure are the input powers from each generator, the output powers to the straps, and the power flowing through the decouplers for a value of R' = 4.1 Ω/m, typical of the usual plasma loading conditions. Note that power flow is negative to line 1.

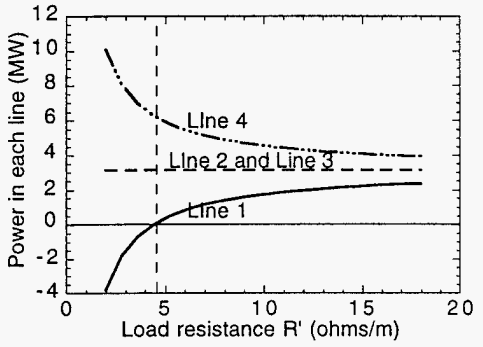

FIGURE 5. Power to each strap vs. R'.

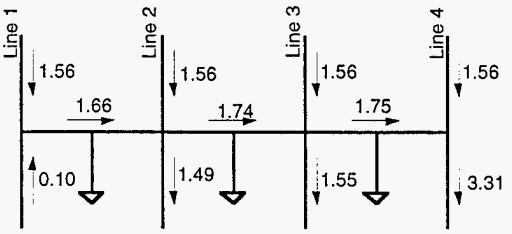

FIGURE 6. Power through decouplers.

Figure 7 shows the voltage and current along transmission lines 1 to 4 vs distance from the connection to the RDL's. The decoupler and the first stub-fast

capacitor pair are connected to the lines 50 m from the RDL; the second stub-capacitor pair is 2.2 m further away. The tuning of the RDL's was changed to compensate for the inter-strap coupling. For strap 4, the RDL was re-tuned to provide a matched load to the 3.31 MW of power to it. This results in a peak voltage on this line of about 14 kV between the antenna and the decoupler, and 17 kV in the 2.2-m length of line between the stubs. The tuning of RDL's 2 and 3 was left unchanged from the uncoupled tuning.

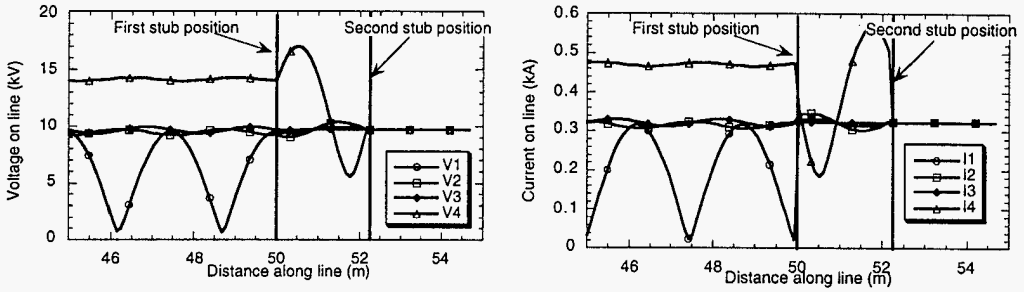

FIGURE 7. Voltage (left) and current (right) in four transmission lines.

Surprisingly, the tuning of the RDL attached to line 1 was also left unchanged from the uncoupled value. As can be seen from the figure, this results in a high VSWR on the segment of line from the RDL to the decoupler, but the peak voltage and current on the line do not exceed the values seen on lines 2 and 3. It is necessary to have voltage on the line at the line-decoupler junction in order to get good power transfer through the decoupler; this tuning allows this to happen.

The results of this analysis indicate peak voltages of $\leq$ 35 kV on the current strap, $\leq$ 45 kV anywhere in the RDL circuit, and $<$ 20 kV in the vacuum and pressurized transmission lines and matching circuitry. The antenna parameters are only slightly higher than present-day experiments, and the transmission line/matching circuit voltages are comparable to those encountered today. With only a modest amount of development and testing of antenna prototypes, it is highly likely that antennas can be built that will operate with these voltages and currents.

3. MECHANICAL ANALYSIS

The ITER environment exposes the antenna to radiated power of 0.25 MW/m^2 under normal conditions, plus an additional 0.25 MW/m^2 for a transient lasting up to 10 s. Since the thermal equilibrium times of the current strap and Faraday shield rods are $\leq$ 10 s, this amounts to the equivalent of a steady-state heat load of 0.5 MW/m^2. In addition, a volumetric power deposition of 15 MW/m^3 at the surface occurs from the neutrons generated during the fusion reaction; for Cu and Fe, this heat flux decays with about a 6-cm e-folding distance.

Two- and three-dimensional thermal and stress analyses have been carried out for the antenna components. Figure 8 shows the temperature contours for a Faraday shield element (5 cm high, 3 cm wide) made of a CuCrZr alloy with 3 mm of Be on the front surface. The resulting thermal stresses (calculated from a 3D NASTRAN analysis) are about 90 MPa.

In addition to the thermal stresses, plasma disruptions will induce eddy currents into the antenna structures. For a disruption typical of those expected for ITER (1), a current of ≈ 60 kA will flow in each Faraday shield tube, which will generate additional forces on the tube ([8]). The results of a 3D NASTRAN analysis of the combined stress case is shown in Fig. 9, and indicates a combined thermal plus disruption stress of ≈ 190 MPa.

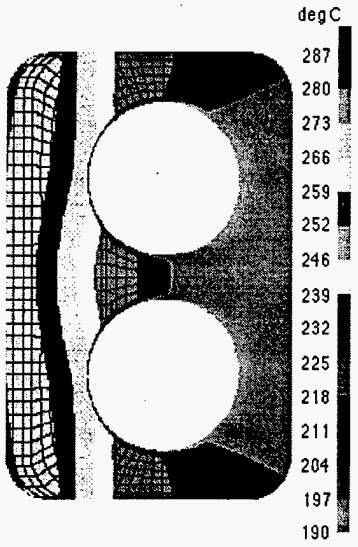

FIGURE 8. Temperature contours in Faraday shield tube.

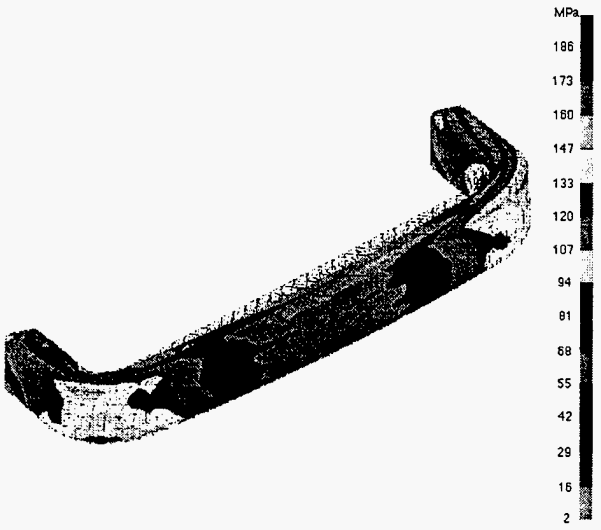

FIGURE 9. Faraday shield stress contours from combined disruption and thermal loads.

Similar stress analyses have been carried out for the current straps, the other critical elements in the antenna structure. If an all-stainless steel current strap is used, thermal stresses up to about 260 MPa are calculated. Thermal stresses for a CuCrZr alloy are much lower, ≤ 100 MPa.

A disruption stress analysis of the current straps has also been done; the results are shown in Fig. 10. The left figure shows the stresses caused by disruption-induced eddy currents flowing in the current strap, and the right figure shows the displacement of the strap. This calculation was done with a 3D electromagnetic model of the antenna structure to allow computation of the time-dependent magnetic field values B(t) along the current strap and pre-matching stubs. Then the currents resulting from the calculated dB/dt were computed and the forces from the interaction of the currents with the machine magnetic field were evaluated; as can be seen, the resulting stress levels were ≤ 130 MPa. Furthermore, they occurred at the corner of the strap, and these values could be reduced considerably by a slight re-design of that particular area.

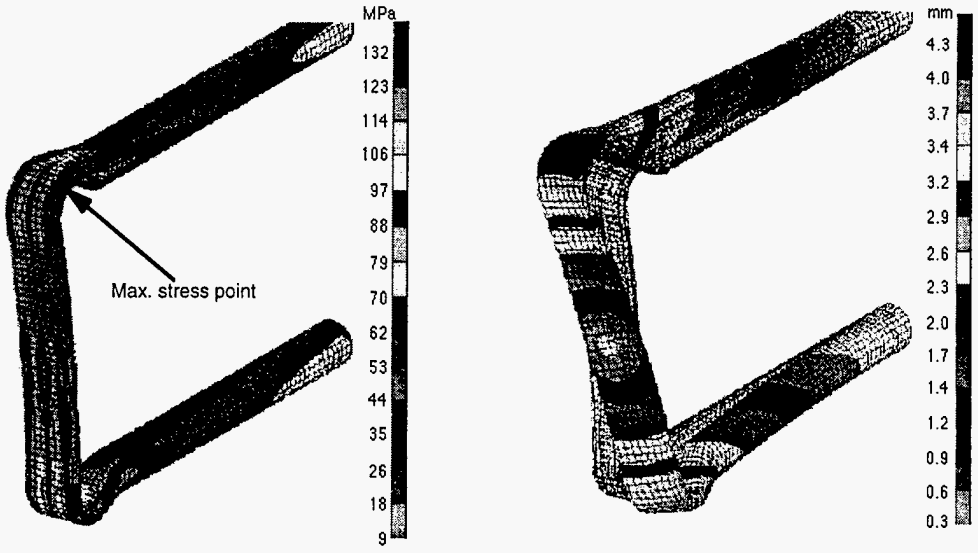

FIGURE 10. Stresses and displacements of stainless steel current strap during a disruption.

A summary of the thermal and stress calculations is given in Table 1, which shows the stress levels calculated for different kinds of loads for a Faraday shield rod and an all-stainless steel current strap. The allowable stress levels were computed using the ITER guidelines (1). For secondary (e.g., thermal) stresses, a value of three times the primary membrane stress (evaluated at the temperature of operation) was used, around 400 MPa for both the CuCrZr alloy and stainless steel. The same value can be used for off-normal events (e.g., disruptions). Although primary membrane stress allowables are much lower, our calculations indicate that the thermal and off-normal allowables tend to be the limiting factors in the design.

TABLE 1. Comparison of calculated vs. allowable stresses in the antenna.

Component	Condition	Stress type	Stress	Allowable
Faraday shield	Normal ops.	Thermal	≈ 90	≈ 400
(CuCrZr alloy)	Disruption	Electromagnetic	≈ 130	≈ 400
	Disruption	Combined	≈ 190	≈ 400
Current strap	Normal ops.	Thermal	≈ 260	≈ 420
(all s. steel)	Disruption	Electromagnetic	≈ 130	≈ 420
	Disruption	Combined	≈ 330*	≈ 420

* Can be lowered with Cu layer on front of strap.

For all case evaluated, the stresses are within limits. The stainless steel current strap has fairly high thermal stresses, which is the major contributor to the 330 MPa combined disruption stress. The use of partial or complete CuCrZr alloy for the current strap reduces the thermal stress levels significantly, but the disruption-induced currents in the CuCrZr are higher than in the stainless steel because of its higher electrical conductivity. Further design work on the current strap, optimizing

the strap shape and the materials, will probably result in a configuration with lower stresses.

4. CONCLUSIONS

An ion cyclotron antenna and matching system has been designed that meets the major criteria for operation and survival in ITER. In particular,

- Voltages only slightly exceed those observed in ICH systems on currently operating tokamaks.
- The matching system can respond to transient changes in plasma loading, achieving a full-power match within ≤ 20 ms
- The generators are protected during very fast transients and should be able to continue high-power operation even in an ELMing discharge.
- Stresses from both normal thermal loads and from disruptions are within the allowable values.

REFERENCES

[1]. ITER Joint Central Team, *ITER General Design Requirements Document* (GDRD), June 1995.

[2]. Hoffman, D. J. et al., "The design of high-power ICRF antennas for TFTR and Tore Supra," in *Applications of Radio-Frequency Power to Plasmas, Seventh Topical Conference, Kissimmee, FL 1987* (AIP Conf. Proc. 159, 1987) p. 302–305.

[3]. Moriyama, S. et al., at "Fourth International Symposium on Fusion Nuclear Technology (ISFNT-4)" April 1997; to be published in special edition of *Fusion Engineering and Design.*

[4]. Durodie, F. "Study of Matching Systems and Schemes for ITER (Design of Fast Tuning Elements)," ITER Design Task D14 Final Report, Nov. 1995.

[5]. Wesner, F. et al., "Experimental Results from ICRF on ASDEX Upgrade," this conference.

[6]. Carter, M. D., et al., "Three-dimensional physics of ICRF launchers for fusion devices," *Nuclear Fusion.* **36**, 209–223 (1966).

[7]. Swain, D. et al., "Preliminary design of in-port ion cyclotron frequency antenna," ITER Design Task D5 Final Report, May 1995. Report no. ITER/US/95/IV-RF-04.

[8]. Swain, D. et al., "Support to ICRF system physics and engineering design," ITER Design Task D320 Final Report, Dec. 1996. Report no. ITER/US/96/IV-RF-05.

Report Number (14) ORNL/CP--94436
CONF-9704102--

Publ. Date (11) 199709
Sponsor Code (18) DOE/ER, XF
JC Category (19) UC-400, DOE/ER

DOE